Wavefront Analysis of Nonlinear Self-Amplified Spontaneous-Emission Free-Electron Laser Harmonics in the Single-Shot Regime

R. Bachelard,[1] P. Mercère,[1] M. Idir,[1] M.-E. Couprie,[1] M. Labat,[1] O. Chubar,[1,2] G. Lambert,[3] Ph. Zeitoun,[3] H. Kimura,[4,5] H. Ohashi,[4,5] A. Higashiya,[4] M. Yabashi,[4] M. Nagasono,[4] T. Hara,[4] and T. Ishikawa[4]

[1]*Synchrotron SOLEIL, L'Orme des Merisiers, Saint-Aubin, BP 48, 91192 Gif-sur-Yvette Cedex, France*
[2]*NSLS-II, BNL, Uton, New York, USA*
[3]*LOA, ENSTA-ParisTech, CNRS-UMR 7639, Ecole Polytechnique, 91761 Palaiseau, France*
[4]*RIKEN, XFEL Project Head Office, Kouto 1-1-1, Sayo, Hyogo 679-5148, Japan*
[5]*Japan Synchrotron Radiation Research Institute, Kouto 1-1-1, Sayo, Hyogo 679-5148, Japan*

(Received 26 October 2010; published 8 June 2011)

The single-shot spatial characteristics of the vacuum ultraviolet self-amplified spontaneous emission of a free electron laser (FEL) is measured at different stages of amplification up to saturation with a Hartmann wavefront sensor. We show that the fundamental radiation at 61.5 nm tends towards a single-mode behavior as getting closer to saturation. The measurements are found in good agreement with simulations and theory. A near diffraction limited wavefront was measured. The analysis of Fresnel diffraction through the Hartmann wavefront sensor hole array also provides some further insight for the evaluation of the FEL transverse coherence, of high importance for various applications.

DOI: 10.1103/PhysRevLett.106.234801 PACS numbers: 41.60.Cr, 42.25.Fx, 42.25.Kb, 42.60.Jf

Thanks to the high degree of transverse coherence of light sources such as synchrotron radiation (SR), free-electron lasers (FEL) [1], and high-order harmonic generation in gas (HHG) [2], the investigation of matter is rapidly evolving together with the development of new imaging methods. Among these techniques, coherent diffraction imaging offers new scales of spatial resolution for both crystals and noncrystallographic samples. First used to reconstruct isolated objects [3,4], the technique was then extended to internal structures in nanosystems [5,6], yeast cells [7], to electronic correlations [8] and from atomic scales [9] to clusters and larger samples [10–12]. Intense, coherent and ultrashort (10–100 fs) vacuum ultraviolet FELs have rapidly emerged such as FLASH in the 80–4.5 nm range [13] and SPring-8 Compact SASE Source (SCSS) Test Accelerator in the 60–40 nm range [14]. X-ray FELs (LCLS [15], XFEL/SPring-8 [16], E-XFEL [17]) open the path to the imaging of biomolecules [18,19] even at atomic scales [5].

In a FEL, a relativistic electron beam wiggling in the periodic permanent magnetic field B_u of an undulator interacts with the electric field of an optical radiation. The wavelength λ of this radiation must equal the undulator resonance wavelength, $\lambda_u(1 + a_u^2)/2\gamma^2$, with $a_u = 0.934 \times B_u[\mathrm{T}] \times \lambda_u[\mathrm{cm}]$, λ_u the period of the undulator magnetic field and γ the normalized electron beam energy. The strong interaction between the high quality electron beam and the optical wave leads to an energy modulation of the electron bunch further converted into a density modulation (microbunching). Several FEL schemes can be implemented. In the self-amplified spontaneous emission (SASE) [20] configuration, the optical wave initially corresponds to the spontaneous emission of the electrons in the undulator magnetic field. The microbunches are uncorrelated and the light emitted has a limited temporal coherence. In the seeding configuration, where the optical wave is an external conventional laser [21,22] or a HHG source [23], the microbunches get correlated, enabling a dramatic improvement of the temporal coherence. The radiation then grows exponentially in the linear regime until saturation when maximum modulation of the electron bunch density is completed. Beyond saturation, in the so-called deep saturation regime, the overmodulation of the electron bunch density reduces the temporal coherence [24]. Each regime is characterized by a specific statistics of the shot-to-shot intensity [25].

The degree of transverse coherence of the FEL radiation increases during the amplification process and can be calculated using the three-dimensional analytical theory [26,27]. A statistical approach [28] enables also to interpret the transverse coherence growth as the emergence of specific TEM modes [29]. Transverse coherence and wavefront quality of the FEL beam are essential not only to probe the FEL physics, but also for user applications requiring tight focusing of light and high illumination on target. Two Young slits experiments enabled the authors of [30,31] to estimate the degree of transverse coherence. Nevertheless, the averaging over few dozens shots was required to counterbalance the pointing instability of the beam, making this experimental approach pointless for single-shot diagnosis. Wavefront analysis using the Hartmann technique was also proposed to assess the spatial characteristics of the FEL source in single-shot regime [32] and also as suitable metrology device for optics alignment [33–35].

In this Letter, we investigate the emission process of a SASE FEL at the SCSS Test Accelerator using a

specifically designed Hartmann Wavefront Sensor (HWS). Single-shot wavefront measurements are performed directly on the FEL giving access to the beam optical quality, the source characteristics and the related instabilities from shot-to-shot. Relevant information about the FEL dynamic are also retrieved at different stages of amplification. Finally, the operation of the HWS in the Fresnel rather than usual Fraunhofer diffraction regime is proposed for further analysis of the FEL transverse coherence.

The SCSS Test Accelerator layout is presented in Fig. 1. The SASE radiation is generated, with a 10 Hz repetition rate, between 61.5 nm and 50 nm wavelengths, by tuning the two undulator gaps. The HWS spatially samples the incident beam with an array of square holes of $l = 150\ \mu$m size each. The resulting beamlets propagate up to a CCD camera, located at a distance $d = 200$ mm behind, leading to individual spots in the detection plane. The wavefront local slopes (i.e. the wavefront derivative values) are retrieved by measuring the positions of these spots centroids with respect to reference positions given by a well-known reference wave. The reconstruction of the wavefront from its local gradients is then based on an iterative algorithm [36]. The reference wave is usually generated by spatial filtering of the incident beam [33,37]. For the present purpose and in order to achieve absolute wavefront measurements of the FEL direct beam, the HWS and the two flat deflection mirrors were first calibrated at 61.5 nm on the nearly perfect spherical part of the wave diffracted by a 50 μm spatial filter pinhole. In this preliminary calibration phase, the accuracy of the sensor could be measured at $\lambda_{\mathrm{VUV}}/125$ Root-Mean-Square (rms) at 61.5 nm.

Figure 2(a) shows a typical Hartmann pattern of a SASE pulse measured at 61.5 nm with the two undulator sections. The beam intensity profile is reconstructed in (b) from the integrated intensity of each luminous spot on the CCD. Figure 2(c) gives the corresponding single-shot phase aberrations in terms of pptical path difference (tilts and focus terms are subtracted). Over 60 successive pulses, the measured mean residual wavefront aberrations are of 3.7 nm rms ($\lambda/17|_{\mathrm{rms}}$) and 17.7 nm peak-to-valley (PV) ($\lambda/3|_{\mathrm{PV}}$), with a standard deviation about 15% over the whole statistics. These measurements show that the optical quality of the SASE fundamental radiation can be optimized below $\lambda_{\mathrm{VUV}}/14|_{\mathrm{rms}}$, which defines the limit of diffraction according to Maréchal's criterion [38], and that imaging and focusing experiments at the limit of diffraction get accessible provided that the further beam line optics involved for spatial conditioning of the FEL beam are also diffraction limited. 0° astigmatism appears as the main residual aberration component, revealing a slight difference between the horizontal and vertical sources longitudinal positions.

Since both intensity and phase profiles of the beam are known from the HWS measurements, Fourier optics backpropagation of the complete electromagnetic field can be performed up to the source location giving access to the FEL source characteristics. Thus, the horizontal and vertical sources could be located, respectively, 2.36 m and 2 m (36 cm distance in between) upstream from the exit of the second undulator, leading to a spread of emission half-angle about $\theta_d = 203\ \mu$rad. Over 60 successive pulses, the source mean sizes are estimated at 73 μm-rms horizontally (with a standard deviation of 4.6 μm) and 72 μm-rms vertically (with a standard deviation of 6 μm).

The SASE FEL radiation emission process and propagation down to the HWS were also simulated using the synchrotron radiation workshop (SRW) [39,40] Fourier propagation code, combined with the GENESIS 1.3 [41] FEL emission code. These simulations [Figs. 2(d)–2(f)] are found to be in good agreement with the experimental measurements [Figs. 2(a)–2(c)] revealing nearly similar Hartmann patterns, intensity and phase profiles, including similar source size, source location and beam divergence.

The study of different configurations of the SASE emission reveals also the evolution of the FEL throughout its different regimes. Indeed, the characteristic length of the SASE FEL exponential growth is $L_g = (2\sqrt{3}k_u\rho)^{-1}$, $\rho = \sqrt[3]{\pi r_e n_0 a_u^2 \Delta_j^2/(4k_u^2\gamma^3)}$ being the Pierce parameter, r_e the classical radius of the electrons, n_0 the electron peak density, $k_u = 2\pi/\lambda_u$ and $\Delta_j = J_0(a_u^2/(2+2a_u^2)) - J_1(a_u^2/(2+2a_u^2))$, where J_n is the Bessel function. In particular, it was shown that for a given undulator period,

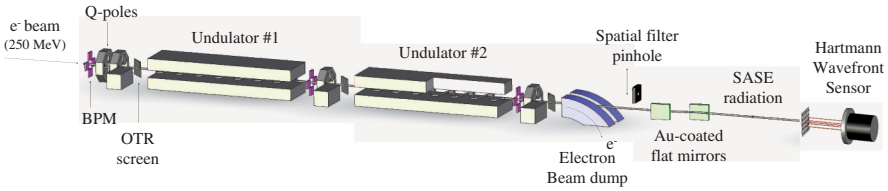

FIG. 1 (color). SCSS test accelerator layout: a 11 m-long 250 MeV accelerator, two in-vacuum undulators (each 4.5 m long, 300 periods of $\lambda_u = 15$ mm) [43], quadrupoles (Q-poles), beam position monitors (BPM) and optical transition radiation (OTR) screens. HWS located at 17.5 m from the end of the second undulator, behind two 5° grazing incidence Au-coated flat mirrors; uniform grid array made out of a 50 μm thick nickel plate and composed of 35×35 square holes (150 μm size squares, rotated by 25° to avoid cross-talking between adjacent spots in the measurement plane, and spaced by 450 μm over a 15.75×15.75 mm^2 effective area); back-illuminated thinned 16-bit XUV detection CCD camera (1024×1024 pixels of 13 μm), coupled to a 10 Hz operating fast shutter and synchronized with the FEL pulse train, allowing for single-shot wavefront measurements.

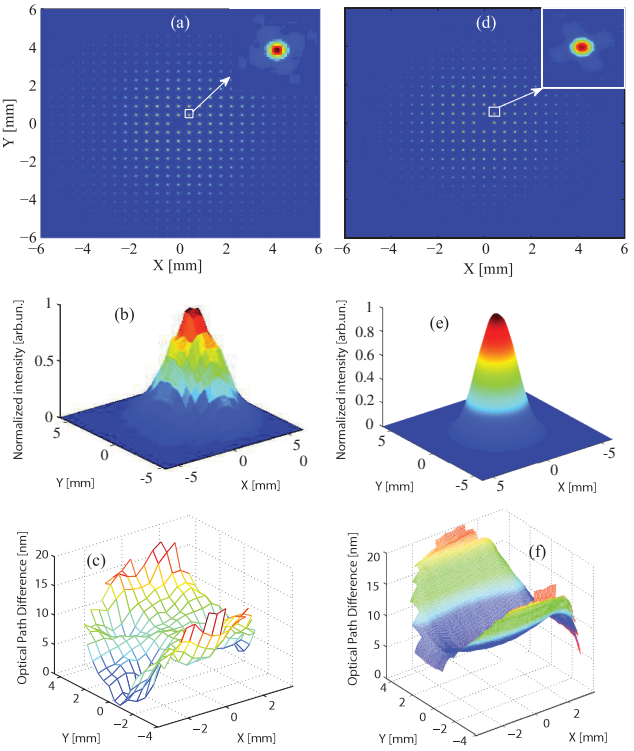

FIG. 2 (color). (a),(d): Hartmann patterns of a single-pulse of the saturated fundamental SASE radiation at 61.5 nm. (b), (e): Respective normalized intensity profiles. (c),(f): Respective phase aberrations given in terms of optical path difference. (a),(b),(c): Experimental data. (d),(e),(f): Simulations performed with GENESIS and SRW (1.43 nm.rad emittance, 0.02% energy spread, 330 A peak current, 0.18 mm-rms bunch length). Because of shot-to-shot beam intensity and size instabilities at the HWS position and for relevant comparison of the wavefront measurements, analysis pupils are limited to $1/e^2$ of the maximum intensity, corresponding to 4σ and 86% of a Gaussian incident flux.

the stage of amplification for the SASE regime depends mainly on the parameter ρN [26], with N the number of undulator periods. At SCSS test accelerator, the saturation occurs for $\rho N \approx 1.1$. Since N is fixed, tuning ρ via the undulator parameter a_u enables to select a given level of amplification. The ρN parameter could also be modified using only one undulator out of the two. Figure 3 shows the measured evolution of the SASE radiation transverse characteristics, intensity fluctuation and power as a function of ρN. As expected from the theory, the intensity fluctuation $\delta I/I$ level significantly reduces after saturation. In addition, the transverse source size is found decreasing up to the saturation regime and increasing after saturation, where the wavefront deteriorates. Indeed, the measurements showed that, at shorter wavelengths, secondary peaks appear in the transverse intensity profile, which probably result from the insufficient number of gain lengths for the TEM_{00} mode to dominate the dynamics [29]. For increasing ρN, the radiation spectral width (not shown here) was measured increasing from spontaneous emission to saturation and decreasing in the deep saturation regime.

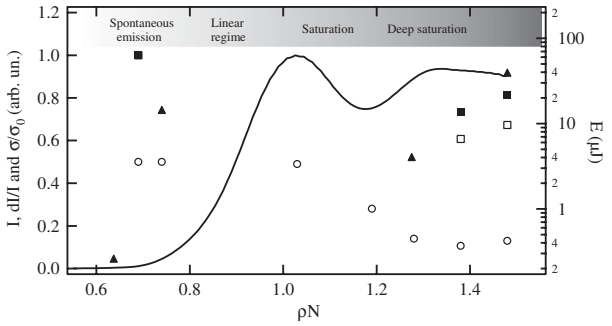

FIG. 3. Measured evolution of the SASE radiation characteristics as a function of ρN: (○) $\delta I/I$ intensity fluctuation measured with a photodiode, (▲) energy (μJ), radiation normalized rms size σ/σ_0 in (□) x and (■) y. Line: calculated normalized energy [26].

The diffraction pattern of the third harmonic ($\lambda_{H3} = 20.5$ nm) through the HWS hole array has also been observed after an aluminum bandpass filter, as illustrated in Fig. 4(a). The pattern exhibits a cloverlike structure, as a result of Fresnel diffraction through a square tilted hole. Indeed, while at 61.5 nm, the Fresnel number $F = l^2/4\lambda d$ is of the order of 0.46, it increases up to 1.37 for the third harmonic, thus violating the far-field approximation of Fraunhofer diffraction. The pattern is well reproduced by simulation with SRW and GENESIS [in (b)]. Figure 4(c) also shows the intensity distribution I that would be expected at the HWS position by considering a fully transversely-coherent radiation (i.e., point source) in the same geometrical configuration. This distribution was calculated using the analytical formula [42] derived in the framework of scalar diffraction theory: $I(x, y) = I_0 D(x\cos\theta - y\sin\theta) D(y\cos\theta + x\sin\theta)$, with

$$D(u) = \left| Erf\left(\frac{e^{-i\pi/4}\sqrt{k}[dl + (l-2u)z_0)]}{2\sqrt{2dz_0(d+z_0)}}\right) - Erf\left(\frac{e^{-i\pi/4}\sqrt{k}[dl + (l+2u)z_0)]}{2\sqrt{2dz_0(d+z_0)}}\right)\right|^2,$$

where k is the radiation wave number and z_0 the distance to the source. The diffraction patterns diagonal cross-sections have been retrieved [Fig. 4(d)–4(f)]. Comparison of the SRW-GENESIS simulation [Fig. 4(e) with dotted line) with the analytical calculation for a point source [Fig. 4(f)], using the same spatial resolution of 1 μm, shows a higher fringe contrast for the fully transversely-coherent radiation. This slight discrepancy opens up interesting possibilities for a deep investigation of the SASE radiation transverse coherence using Fresnel diffraction from many holes. In particular, this method potentially enables reconstruction of the entire transverse autocorrelation function over the total wavefront at once, for a single SASE pulse, which is not possible with other methods. Since, with appropriate choice of the HWS parameters, there is no cross interference of radiation from different holes, the

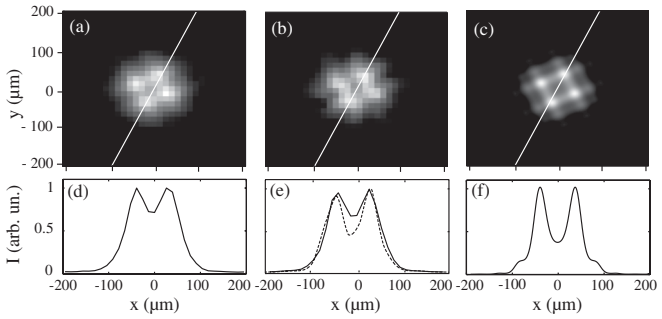

FIG. 4. HWS diffraction pattern of a single-pulse of the SASE radiation third harmonic at 20.5 nm: (a) experimental measurement, (b) SRW-GENESIS simulation using the experimental spatial resolution (13 μm), (c) analytical calculation considering a fully coherent wave (point source) and using a 1 μm spatial resolution. (d),(e) and (f) Respective diagonal cross-sections (along the white lines). (e) continuous line using the experimental CCD 13 μm resolution, dotted line using the analytical calculation 1 μm resolution. HWS set with holes of 150×150 μm. Spectral selection with a 500 nm thick oxidized aluminum filter.

reconstruction algorithm can be relatively simple: it can be based on the analysis of individual diffraction patterns from each hole. For qualitative analysis of the degree of coherence variation over the wavefront, comparison of the fringe contrast in diffraction patterns from individual holes with that of the fully transversely coherent case can be used. Such a HWS signal could then be used to optimize the transverse coherence by adjusting the gain length.

In summary, single-shot SASE wavefront measurements of the SCSS Test accelerator have been performed with a specifically designed Hartmann wavefront sensor. Measurements enabled complete characterization of the source and demonstrated the high optical quality of the beam ($\lambda/17|_{\mathrm{rms}}$ with a standard deviation about 15% from shot-to-shot). An increase in stability of the radiated intensity as well as a slight decrease of the temporal coherence and transverse structure were demonstrated, providing a further insight in the coupled evolution of the longitudinal and transverse FEL dynamics during amplification and saturation. Finally, the Fresnel diffraction patterns observed for the third harmonic of the FEL radiation were shown to contain information about the degree of transverse coherence of the source. Such an observation can be easily obtained with the fundamental radiation as well.

The authors acknowledge the SCSS Test Accelerator team at RIKEN, Imagine Optic Company, IA-SFS, and Triangle de la Physique (CLEL, SAX2, FEASO).

[1] D. A. Deacon *et al.*, Phys. Rev. Lett. **38**, 892 (1977).
[2] M. Lewenstein *et al.*, Phys. Rev. A **49**, 2117 (1994).
[3] J. Miao *et al.*, Proc. Natl. Acad. Sci. U.S.A. **100**, 110 (2002).
[4] H. N. Chapman, Nature Phys. **2**, 839 (2006).
[5] I. K. Robinson, Phys. Rev. Lett. **87**, 195505 (2001).
[6] M. A. Pfeifer, Nature (London) **442**, 63 (2006).
[7] D. Shapiro *et al.*, Proc. Natl. Acad. Sci. U.S.A. **102**, 15 343 (2005).
[8] D. Le Bolloc'h *et al.*, Phys. Rev. Lett. **100**, 096403 (2008).
[9] K. J. Gaffney and H. N. Chapman, Science **316**, 1444 (2007).
[10] B. Abbey *et al.*, Nature Phys. **4**, 394 (2008).
[11] R. L. Sandberg, Phys. Rev. Lett. **99**, 098103 (2007).
[12] A. Ravasio *et al.*, Phys. Rev. Lett. **103**, 028104 (2009).
[13] W. Ackermann, Nat. Photon. **1**, 336 (2007).
[14] T. Shintake *et al.*, Nat. Photon. **2**, 555 (2008).
[15] Z. Huang *et al.*, Phys. Rev. ST Accel. Beams **13**, 020703 (2010).
[16] T. Shintake *et al.*, *Proc. of EPAC'06* (Edinburgh, Scotland, 2006).
[17] R. Brinkmann *et al.*, *Proc. of the FEL'06* (Berlin, Germany, 2006).
[18] R. Neutze *et al.*, Nature (London) **406**, 752 (2000).
[19] M. Bergh, N. Tîmneanu, and D. van der Spoel, Phys. Rev. E **70**, 051904 (2004).
[20] A. M. Kondratenko and E. L. Saldin, Sov. Phys. Dokl. **24**, no. 12, 986 (1979); R. Bonifacio *et al.*, Opt. Commun. **50**, 373 (1984); K.-J. Kim, Phys. Rev. Lett. **57**, 1871 (1986).
[21] R. Prazeres *et al.*, Nucl. Instrum. Methods Phys. Res., Sect. A **272**, 68 (1988).
[22] A. Doyuran *et al.*, Phys. Rev. Lett. **86**, 5902 (2001).
[23] G. Lambert *et al.*, Nature Phys. **4**, 296 (2008).
[24] A. H. Lumpkin *et al.*, Phys. Rev. Lett. **88**, 234801 (2002).
[25] E. L. Saldin *et al.*, Opt. Commun. **281**, 1179 (2008).
[26] K.-J. Kim, Phys. Rev. Lett. **57**, 1871 (1986).
[27] G. Geloni *et al.*, New J. Phys. **12**, 035021 (2010).
[28] J. W. Goodman, *Statistical Optics* (Wiley, New York, 1985).
[29] M. Xie, Nucl. Instrum. Methods Phys. Res., Sect. A **445**, 59 (2000).
[30] R. Ischebeck *et al.*, Nucl. Instrum. Methods Phys. Res., Sect. A **507**, 175 (2003).
[31] A. Singer, Phys. Rev. Lett. **101**, 254801 (2008).
[32] P. Mercère *et al.*, *Proc. of the FEL'09 Conf.* (Liverpool, Scotland, 2009), p. 702.
[33] P. Mercère *et al.*, Opt. Lett. **28**, 1534 (2003).
[34] M. Kuhlmann *et al.*, *Proc. FEL'06* (Berlin, Germany, 2006).
[35] B. Floter *et al.*, Nucl. Instrum. Methods Phys. Res., Sect. A **635**, S108(2011).
[36] W. H. Soutwell, J. Opt. Soc. Am. **70**, 998 (1980).
[37] J. Gautier *et al.*, Eur. Phys. J. D **48**, 459 (2008).
[38] A. Maréchal, Revue d'Optique, Theorique et Instrumentale **26**, 257 (1947).
[39] O. Chubar and P. Elleaume, *Proc. EPAC'98*, p. 1177 (1998).
[40] M. Bowler, J. Bahrdt, and O. Chubar, *Modern Developments in X-Ray and Neutron Optics* (Springer, Berlin, 2008), Vol. 137, p. 69.
[41] S. Reiche, Nucl. Instrum. Methods Phys. Res., Sect. A **429**, 243 (1999).
[42] E. Hecht, *Optics* (Addison Wesley, Farmington Hills, MI, 1987), 2nd ed.
[43] T. Shintake *et al.*, Nat. Photon. **2**, 555 (2008).